Electrostriction of near-critical SF_6 in microgravity

G. A. Zimmerli,[1] R. A. Wilkinson,[2] R. A. Ferrell,[3] and M. R. Moldover[4]

[1]*National Center for Microgravity Research, Cleveland, Ohio 44135*

[2]*Microgravity Science Division, NASA Lewis Research Center, Cleveland Ohio 44135*

[3]*Department of Physics, University of Maryland, College Park, Maryland 20742*

[4]*Physical and Chemical Properties Division, NIST, Gaithersburg, Maryland 20899*

We used interferometry to measure the electric-field-induced (*i.e.*, "electrostrictive") increase of the density of sulfur hexafluoride near its critical point. The results at the temperatures $T_c + 5$ mK, $T_c + 10$ mK, and $T_c + 30$ mK with $T_c = 319$ K agree with a calculation based on the Clausius-Mossotti relation and the restricted cubic model equation of state. These measurements were performed in microgravity so that the electrostrictive density changes (≤ 3.5 % in this work) would not be complicated by stratification of the fluid's density induced by the Earth's gravity.

PACS numbers: 51.50.+v, 05.70.Jk, 51.35.+a, 64.30.+t

Some prior studies of electric field effects near liquid-vapor critical points used weak fields to successfully detect the dielectric constant anomaly[1-5], while others have used strong fields in searches for field-induced shifts of the consolute temperatures of binary liquid mixtures[6-8]. The binary mixtures are easily handled; however, they are imperfect insulators. The applied field inevitably leads to ohmic heating that prevents the study of electric field effects *at equilibrium.* Here, we applied fields up to 26 kV/cm to non-conducting, pure sulfur hexafluoride (SF_6), near its liquid-vapor critical point. We measured the electric-field-induced increase of the density of the SF_6 in equilibrium at the temperatures T_c + 5.0 mK, T_c + 10.0 mK, and T_c + 30.0 mK, where T_c = 319 K is the critical temperature. The density increase was as large as 3.5%, and it agreed with the published equation of state. This agreement establishes the feasibility of a proposal to measure the equation of state even closer to a liquid-vapor critical point in microgravity by measuring a pure fluid's response to weaker electric fields[9].

The density increase was an example of the deformation of a fluid by the presence of an electric field, which we call "electrostriction" in analogy with those electric-field-induced deformations of a solid which are independent of the reversal of the field direction. Near a critical point, electrostriction becomes more pronounced because of the diverging isothermal compressibility. The present work extends the electrostriction measurements made by Hakim and Higham[10] on liquids to a near-critical fluid which had an isothermal compressibility 10^7 times larger.

Starting from the electrical force equation, Stratton[11] shows that the relation between electrical pressure P_E and electric field E for a fluid in equilibrium is:

$$\int_0^{P_E} \frac{dP_E}{\rho} = \frac{1}{2}\varepsilon_0 E^2 \frac{d\kappa}{d\rho} \qquad (1)$$

where ε_0 is the vacuum permittivity, ρ the fluid density, and κ the dielectric constant ($\kappa = 1.28$ for SF_6 at the critical density). For an incompressible fluid the electrical pressure is given by

$$P_E = \varepsilon_0 E^2 (\kappa - 1)(\kappa + 2)/6 \qquad (2)$$

when the Clausius-Mossotti relation connects the dielectric constant to the density. When a compressible fluid, such as SF_6 near the critical point, is subjected to an electric field, there is an accompanying change of its density that can be calculated from Eq. (1) and the fluid's equation of state. In the limits of a linear response and isothermal conditions, the density change due to electrostriction is $\Delta\rho/\rho = \beta_T P_E$ where β_T is the isothermal compressibility.

Earth-based measurements of the electrostriction effect near the liquid-vapor critical point are completely masked by gravity effects. The scale of gravity effects can be compared to electrostriction by noting that the gravitationally caused pressure gradient in SF_6 at its critical density (730 kg/m^3) is $2.9\times10^{-6} P_c$ per millimeter of height, where P_c is the critical pressure. Thus, the gravitational pressure difference across an SF_6 sample only 0.12 mm high equals the electrical pressure produced by an electric field of 10 kV/cm. Furthermore, in the Earth's gravity, the density-stratified, near-critical SF_6 would experience a force from an applied electric field, even if electrostriction were negligible. By performing the experiment in a microgravity environment, we were able to avoid density stratification in the sample and thus make an accurate measurement of the electrostriction effect.

The experiment was carried out using the Critical Point Facility[12] (CPF) which flew on the Second International Microgravity Laboratory (IML-2) mission during the STS-65 Mission of the Space Shuttle Columbia during 1994. As described in greater detail in another publication[13], the CPF thermostat stabilized the temperature of the sample cell to within 0.1 mK for intervals of many hours.

A schematic diagram of our sample cell is shown in Figure 1. The sample cell was filled to within 0.3% of the critical density with 99.999% pure SF_6. The heart of the cell was a coin-shaped volume of SF_6 that was studied by interferometry. The SF_6 was confined by two flat quartz windows and by a washer-shaped stainless-steel spacer. The inside diameter of the spacer was 12 mm, and its thickness was 2 mm. Approximately one quarter of this confined volume was occupied by a 1 mm-thick, semicircular, quartz "button" attached to one window.

The interferometer sample cell comprised one leg of a Twyman-Green interferometer. A multi-layer dielectric mirror coated the inner surface of one of the windows. Both surfaces of the other window had anti-reflection coatings. In addition to the optical coatings, both inner surfaces of the windows were coated with a conductive, transparent, indium-tin-oxide film. The conductive films on the inner window surfaces and the spacer were electrically grounded throughout the experiment. A 0.125 mm diameter wire passed through the 2 mm thick section of the SF_6 parallel to the edge of the quartz button and 1.8 mm away from its edge. The wire was charged to 500 V to apply an inhomogeneous electric field to the sample.

Figure 2 shows the equilibrium fringe pattern that developed during a 14 hour-long interval while the wire was charged to a potential of 500 V at T_c + 5.0 mK. Before the wire was charged, the fringes near the wire had been straight. After the wire was charged, the density of the SF_6 near the wire gradually increased because of electrostriction and the fringes developed cusp-like curvature on both sides of the wire. Because the thermal diffusivity of the SF_6 approaches zero

near the critical point, it was necessary to wait increasingly long times for the electrostriction fringe pattern to reach equilibrium. Interferograms similar to that in Figure 2 were also obtained at T_c + 30.0 mK, and T_c + 10.0 mK, after waiting 3 and 6 hours respectively.

Far from the wire, the fringe pattern was determined primarily by the tilted reference mirror of the interferometer and by the distortion of the cell's windows; these effects were evident even at T_c + 1 K when the electric field was turned off.

The electric field produced by a charged wire passing halfway between two grounded parallel plates separated by a distance l is

$$E^2 = \frac{C^2V^2}{2l^2\varepsilon_0^2}\left(\cosh\left(\frac{2\pi x}{l}\right)-\cos\left(\frac{2\pi z}{l}\right)\right)^{-1} \tag{3}$$

where the x-axis is perpendicular to the wire and parallel to the grounded window surfaces, and the z-axis is perpendicular to the windows. In Eq. (3), V = 500 V is the voltage applied to the wire, $C = 2\pi\varepsilon_0/[\ln(2l/\pi a)]$ is the wire's capacitance per unit length and a is the wire's radius. The maximum electric field occurred at the surface of the wire and was 26 kV/cm. Because of the screening by the grounded windows, the electric field decreased rapidly with distance becoming 1 kV/cm at x = 1 mm.

The isothermal compressibility $\beta_T = (1/\rho)(\partial\rho/\partial P)_T$ diverges on the critical isochore near the critical point as $\beta_T = \Gamma t^{-1.24}/P_c$ where $t = (T - T_c)/T_c$ is the reduced temperature, and Γ = 0.0459 for SF_6 in the restricted cubic model[14]. With the wire charged to a 500 V potential, the electrical pressure P_E at the surface of the wire was $2.4\times10^{-6}\ P_c$. Although this is a relatively small pressure increase, the compressibility is large enough near the critical point that P_E induces a nonlinear

density change. Close to the wire, and within about 20 mK of the critical temperature, β_T can not be approximated by a function of the temperature alone, *i.e.* independent of P_E. Thus, it was necessary to use Eq. (1) together with the equation of state of SF_6 to numerically compute the density increase on each isotherm due to P_E. Figure 3 shows the density change as a function of pressure, normalized to values at the critical point, as calculated from the restricted cubic model parameters found in Ref. 14.

Changes in the density near the wire were determined from the fringe pattern. The nominal optical path of the laser light in the fluid was $N\lambda = 2ln$. Here, N is the number of wavelengths required to pass twice through the fluid, $\lambda = 633$ nm was the wavelength of the light in vacuum, $l = 2$ mm was the thickness of the fluid, and $n = 1.092$ is the index of refraction of the SF_6 at the critical density[17]. The change in optical path length of a ray passing through the fluid is calculated by integrating the density increase along the light path. The change in fringe order at a lateral distance x from the wire is then given by

$$\Delta N(x) = \frac{2}{\lambda} n' \int_{-l/2}^{l/2} \frac{\Delta\rho(x,z)}{\rho} dz. \qquad (4)$$

where $n' = \rho dn/d\rho = (n^2 - 1)(n^2 + 2)/6n$ is obtained from the Lorentz-Lorenz relation connecting the density to index of refraction. In the linear regime, the compressibility is independent of position and the integral can be evaluated analytically. However, at temperatures close to T_c and for small x, it is necessary to compute the integral numerically. The resolution of the measurements was $\Delta N = 0.03$ fringes corresponding to a density resolution of 0.005 % in the 2 mm thick section of the SF_6 sample.

Because of the periodic nature of the fringe pattern, the image analysis is well suited to Fourier-transform analysis. A density increase near the wire due to electrostriction produces a change in the phase of the fringe pattern; however, the spatial frequency of the fringe pattern parallel to the wire remains unchanged.

The Fourier analysis of interferograms at several temperatures showed that far from the wire, where the electrostrictive density changes were always small, the phase data for different temperatures did not coincide. Thus, there was a spurious temperature and/or time dependence to background fringe pattern, upon which the near-cusp was superimposed. Such a dependence might have been caused by creeping motion of one or more of the optical components within CPF. The analysis compensated for this spurious dependence of the fringe patterns by subtracting the phase data at $T_c + 1$ K from the other sets of phase data and by adding to each result a constant chosen to yield zero phase shift far from the wire.

We expected the fringe shift due to electrostriction to be symmetrical on both sides of the wire. However, the typical fringe pattern had a small (< 0.2 fringe) asymmetry. The asymmetry was consistent with a slight rotation of the background fringe pattern and it was detected even far from T_c. The final data analysis eliminated the effect of the rotation by averaging data from the two sides of the wire.

Because the CPF interferometer optics had not been focused at the sample cell, an additional correction was needed to account for the effect of refraction. Using detailed data about the interferometer optical train[15] we calculated that the distance from the sample cell to the imaging plane was $z_0 = 6.6$ cm.

The effect of refraction on the interferograms is twofold. First, a refracted ray is displaced from its "true" position. The refracted ray carries phase information from the lateral coordinate x_0

where it exits the sample cell, to a new position $x_0' = x_0 + z_0\tan\theta$ at the imaging plane. (Here θ is the angle the refracted ray subtends with the normal.) For example, a ray passing close to the left side of the wire in the cell can be refracted to the right side of the wire at the imaging plane. Large magnified images of the interferograms were used to manually trace the faint, extended, images of fringes that originated from the opposite side of the wire. Fringe shift data from the manually traced fringes were appended to the Fourier transform data. The two methods of analysis yielded data that matched smoothly in the vicinity of the wire.

A second consequence of refraction is the addition of optical path length. A ray that exits the fluid at an angle θ travels an extra distance relative to a ray that is not refracted. The additional path length traveled by the refracted ray increases the phase by the amount $\pi\theta^2 z_0/\lambda$. The angle θ that the refracted ray subtends with the normal is calculated from the expression $\sin\theta = (\lambda/2\pi)(d\varphi/dx)$, where φ is the phase of the wavefront in the plane $z_0 = 0$ where the wavefront exits the fluid.

Figure 4 compares the measured fringe shifts due to electrostriction with theory, as a function of distance x from the wire and of temperature. The solid curves are the theoretical shifts that account for the non-linearity of the compressibility and the effect of refraction. The agreement between theory and experiment is excellent; the differences are within the noise of the fringe-shift measurements, which is approximately 0.03 fringes near the wire. (The uncertainty stated is a single standard uncertainty, *i.e.* the coverage factor k=1.) At T_c + 5.0 mK, the fluid density ranges from ρ_c far from the wire, to $1.035\rho_c$ close to the wire. The data for $x > 0$ are from the Fourier transform analysis of the fringe patterns, and the data for $x < 0$ data are from hand-traced fringes. The only parameter used in the data analysis is the small phase shift added to the Fourier transform data to require the fringe shift to be zero far from the wire.

In Fig. 4, the dashed curves indicate the fringe shifts from a calculation that accounts for the nonlinear compressibility; however it neglects refraction. In effect, refraction maps the points on the dashed curve to points in the solid curve; thus, refraction has a major influence on the fringe pattern close to the wire. Using the restricted cubic model equation of state for SF_6 and accounting for the effect of refraction on the out-of-focus interferometric images obtained in a microgravity environment, we obtained quantitative agreement between electrostriction theory and data for a highly compressible fluid.

We thank R. Gammon, H. Hao, R. Kusner, W. Johnson, M. Bayda, H. Nahra and the entire CPF team for participating in the experiment operations. We are grateful to NASA, ESA, and the STS-65 crew who made this experiment possible. We thank K.Y. Min and J. K. Bahattacharjee for useful discussions. This work was supported by NASA through its Microgravity Science and Applications Division.

References

1. R. Hocken, M. A. Horowitz, and S. C. Greer, Phys. Rev. Lett. **37**, 964 (1976).
2. B. J. Thijsse, J. Chem. Phys. **74**, 4678 (1981).
3. M. W. Pestak and M. H. W. Chan, Phys. Rev. Lett. **46**, 943 (1981).
4. J. L. Tveekrem, S. C. Greer, and D. T. Jacobs, Macromolecules **21**, 147 (1988).
5. J. Hamelin, B. R. Gopal, T. K. Bose, and J. Thoen, Phys. Rev. Lett. **74**, 2733 (1995).
6. P. Debye and Kleboth, J. Chem. Phys. **42**, 3155 (1965).
7. Y. Yosida, Phys. Lett. **65A**, 161 (1978).
8. D. Wirtz and G. G. Fuller, Phys. Rev. Lett. **71**, 2236 (1993).
9. M. Barmatz, Preliminary NASA Science Requirements Document, "Microgravity Scaling Theory Experiment," unpublished (Nov. 13, 1996).
10. S. S. Hakim and J. B. Higham, Proc. Phys. Soc. **80**, 190 (1962).
11. J.A. Stratton, *Electromagnetic Theory*, Chap. 2 (McGraw-Hill, New York, 1941).
12. M. Cork, T. Dewandre, and D. Hueser, ESA Bulletin **74**, 36 (1993).
13. R. A. Wilkinson, G. Zimmerli, H. Hao, M. R. Moldover, R. F. Berg, W.L. Johnson, R. A. Ferrell and R. W. Gammon, Phys. Rev. E **57**, 436 (1998).
14. M.R. Moldover, J.V. Sengers, R.W. Gammon, and R.J. Hocken, Rev. Mod. Phys. **51**, 79 (1979).
15. T. Dewandre kindly provided data regarding the CPF optics.

Figure Captions

FIG. 1. The sample cell. The fine wire passing through the SF_6 was charged to 500 V to generate the electric field.

FIG 2. Interferogram of the SF_6 fluid in a low gravity environment at $T_c + 5.0$ mK after 14 hr at 500 V. The bending of the fringes near the wire signifies the density increase due to the electrostriction effect. The discontinuity in the fringe pattern across the diameter of the cell shows the change of the optical path at the edge of the quartz button.

FIG 3. The relative density as a function of the relative pressure of SF_6. The calculated curves used the restricted cubic model. When the wire was charged to 500 V, the electrical pressure at the surface of the wire was $2.4\times10^{-6}\ P_c$, as indicated by the dashed line.

FIG 4. Measured electrostriction fringe shift in SF_6 as a function of distance x from the center of the wire: $T_c + 5.0$ mK (O); $T_c + 10.0$ mK (∇); and $T_c + 30.0$ mK ($\square$). The solid curves are calculated fringe shifts that include the nonlinear response of the SF_6 and the effects of refraction. The dashed curves include nonlinearity but neglect refraction; thus, they have cusps at $x = 0$.

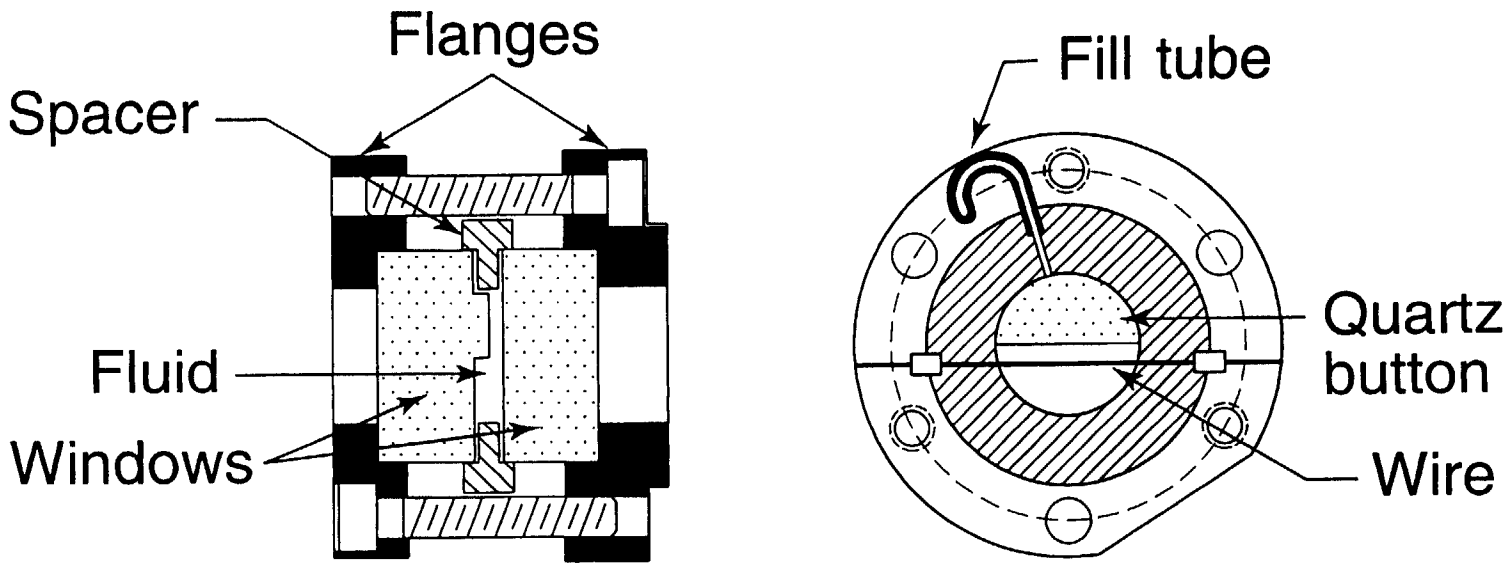

Figure 1


ERT: 295175 S
= 4419 M
EXP: AFEQ
MET:7/14:45:1
TEMP: 45.5349 deg C
GMT:197 / 28881
GMT:197 /7:38:1

Figure 2

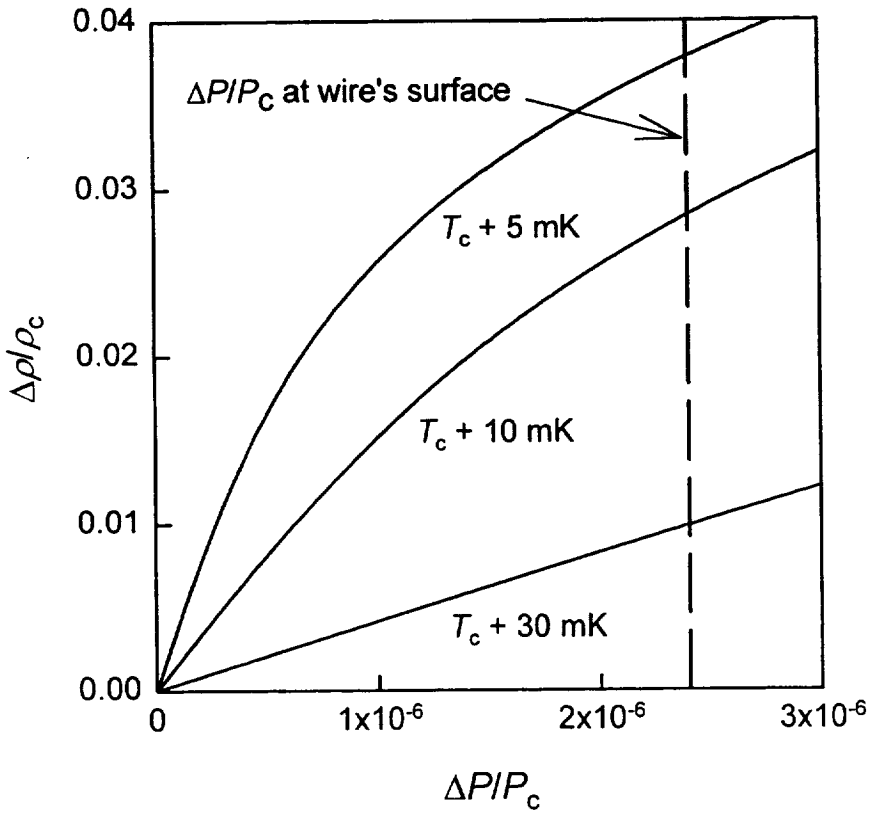
0.04
0.03
0.02
0.01
0.00
$\Delta\rho/\rho_c$
$\Delta P/P_c$ at wire's surface
T_c + 5 mK
T_c + 10 mK
T_c + 30 mK
0
1x10^{-6}
2x10^{-6}
3x10^{-6}
$\Delta P/P_c$

Figure 3

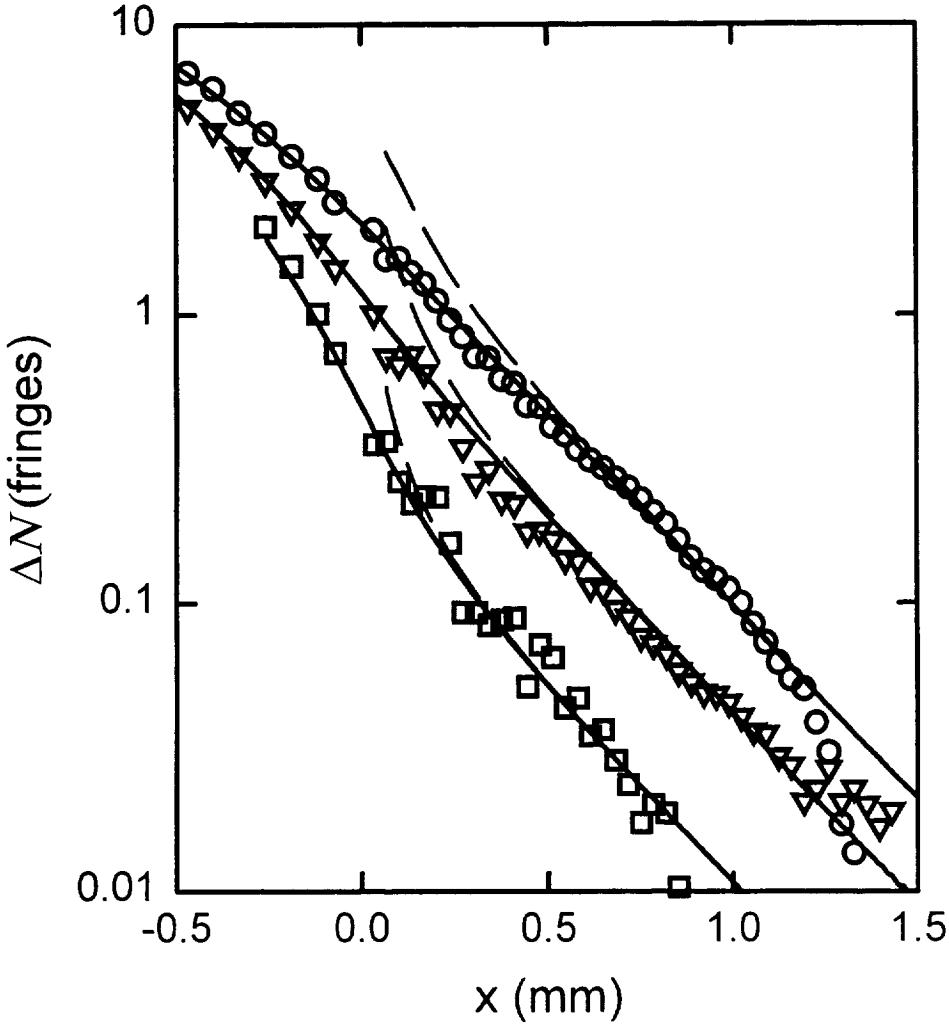

Figure 4